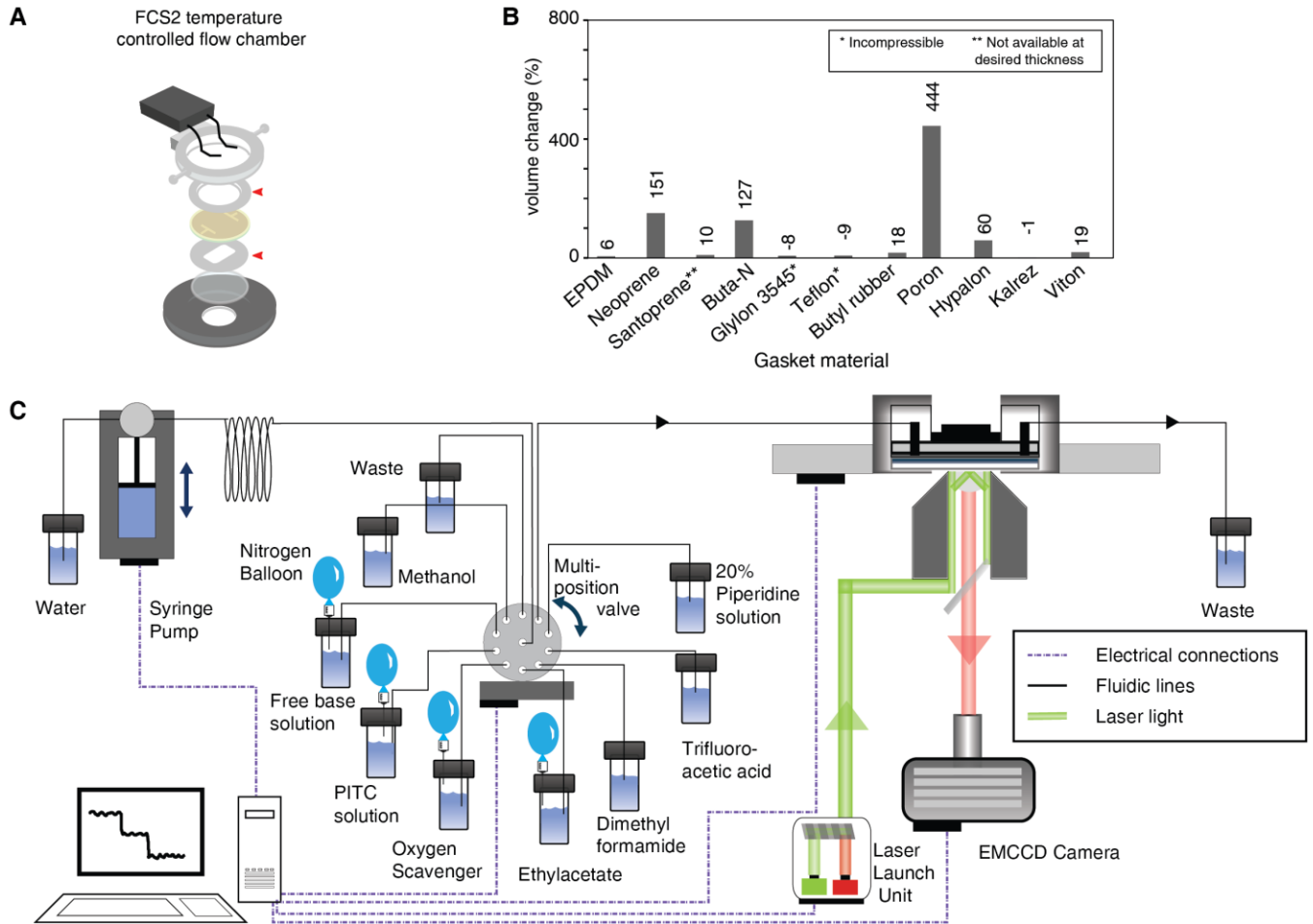**Supplementary Figure 1**

Only select fluorophores exhibit fluorescence stability toward Edman reagents.

(**A**) Fluorophores (spanning four fluorescent channels, denoted by bar colors) were tested for their percentage change in fluorescence intensity in PBS buffer, following a 24 hour incubation with TFA or pyridine/PITC (shown as pyridine). Dyes marked with boxes exhibited only moderate changes (<20%) in fluorescence. The data are presented as mean across replicates, shown, with error +/- s.d. where $n \geq 3$. (**B**) Images of fluorophore coupled Tentagel beads illustrate fluorescence changes by Edman reagents. In the case of BODIPY-FL (left panels), the fluorescence intensity decreases with TFA incubation, while there is a spectral redshift with pyridine incubation. In contrast, Atto647N (right panels) is stable in both color and intensity to both conditions. Scale bar, 200μm.

A FCS2 temperature controlled flow chamber

B volume change (%) vs Gasket material

* Incompressible   ** Not available at desired thickness

Gasket material	volume change (%)
EPDM	6
Neoprene	151
Santoprene**	10
Buta-N	127
Glylon 3545*	-8
Teflon*	-9
Butyl rubber	18
Poron	444
Hypalon	60
Kalrez	-1
Viton	19

C — Water, Syringe Pump, Nitrogen Balloon, Methanol, Waste, Multi-position valve, 20% Piperidine solution, Free base solution, PITC solution, Oxygen Scavenger, Ethylacetate, Dimethyl formamide, Trifluoro-acetic acid, Laser Launch Unit, EMCCD Camera, Waste

--- Electrical connections
— Fluidic lines
— Laser light

Supplementary Figure 2

Adaptation of flow-cell, TIRF-microscopy, and computer-controlled fluidic system for Edman sequencing.

We modified a Bioptechs FCS2 perfusion chamber (**A**) for Edman sequencing by substituting the silicone gaskets as indicated by red arrows, with perfluoroelastomer gaskets resistant to the Edman chemistry. (**B**) Eleven different polymeric materials sourced through a number of vendors were cut into 2cm x 1cm strips and tested for inertness following 24 hours of TFA incubation. Kalrez-0040 showed the least change in volume, excellent inertness to pyridine/PITC, and good compressibility (shore durometer A = 70); we used it for all subsequent experiments. Teflon (polytetrafluoroethylene) gaskets, although suitably inert, were not compressible and caused leaks when used in the perfusion chamber. Image of flow chamber is adapted from vendor (Bioptechs) supplied image. (**C**) Edman sequencing was implemented using a syringe pump (3-way valve configuration) and a 10-port multi-position valve system automated to exchange solvents through polytetrafluoroethylene tubing into the imaging perfusion chamber attached to the stage of a TIRF microscope.
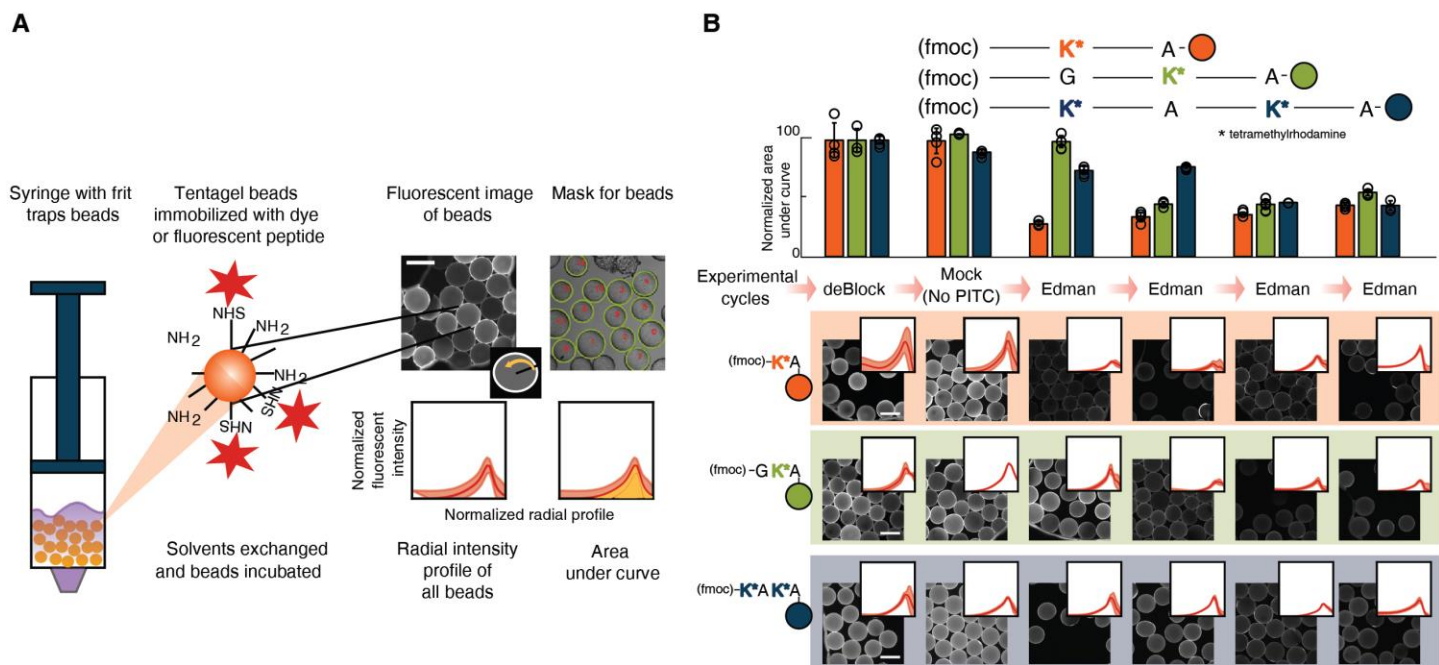
Supplementary Figure 3

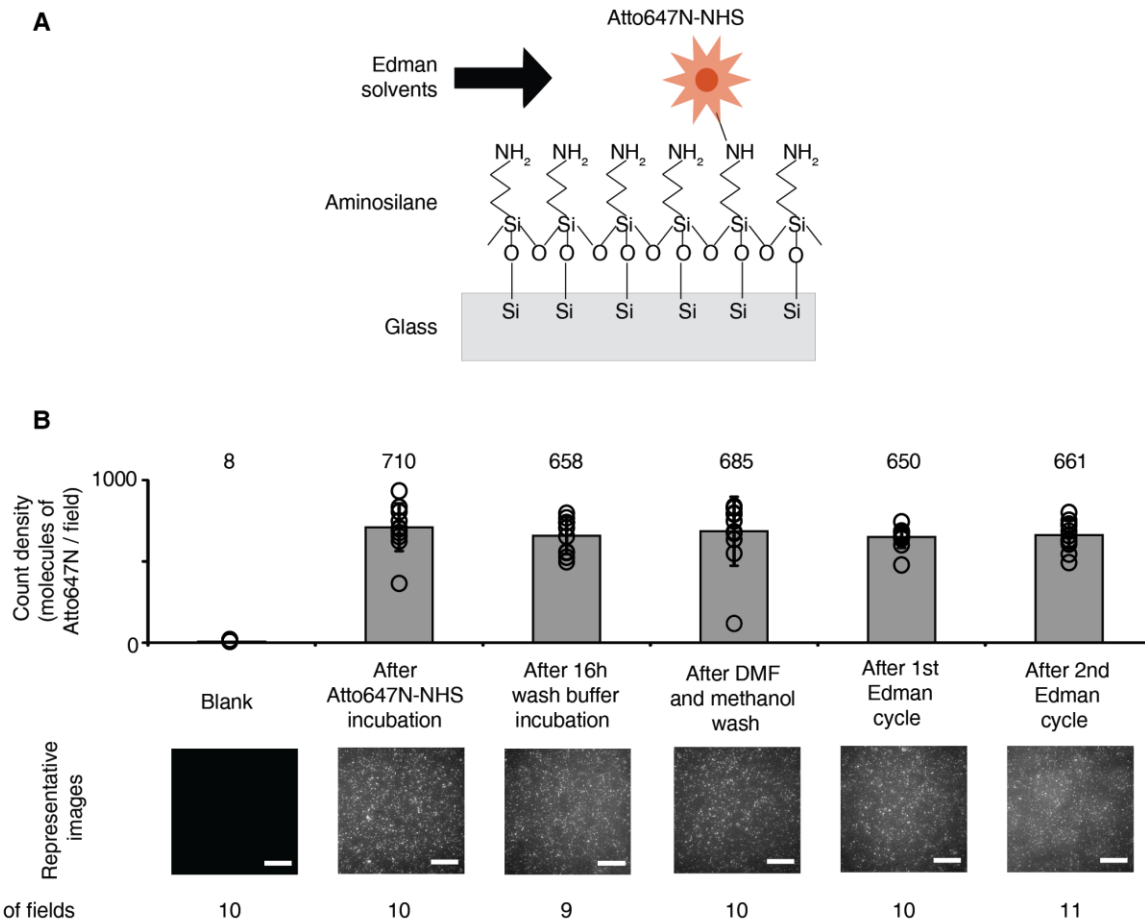Bead-based assays confirm bulk Edman sequencing of fluorescently labeled amino acids.

(**A**) Specific binding of TMR to functionalized Tentagel beads occurs at the periphery and density can be measured by image processing. Peripheral bead fluorescence intensities were calculated by computing the area under the fluorescence intensity radial distribution normalized relative to a negative control beads bound non-specifically with free TMR lacking the NHS group to control for background fluorescence. (**B**) Edman degradation can be used to determine the positional information of the fluorescently labeled lysine residues of synthetic peptides using bulk fluorescence measurements. Bar charts indicate the normalized average of the fluorescence intensity per bead +/- s.d. across image fields. Raw fluorescence intensities and field counts are reported in **Supplementary File 1.**
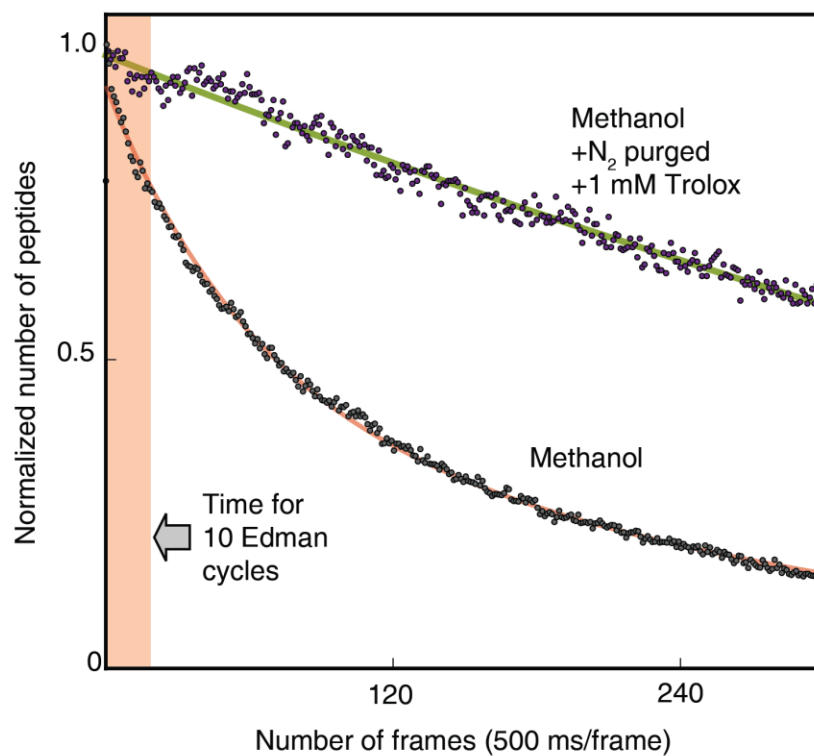
Supplementary Figure 4

Nitrogen-purged methanol with Trolox significantly decreases photobleaching and fluorophore blinking.

Fluorescence loss is greatly reduced for the TMR labeled peptide, (fmoc)-K*A, under constant laser illumination in nitrogen purged 1 mM Trolox in methanol (top, green, curve, n=2802) versus imaging in methanol alone (bottom, red, curve, n=5942), imaged with consecutive 0.5 sec frames. Solid lines represent fits of each data set to a single exponential. Imaging in methanol/Trolox resulted in a $t_{1/2}$ of approx. 105 seconds. * indicates TMR conjugated to lysine. Solid lines represent fits to single exponential decay functions.

A

Atto647N-NHS

Edman solvents

Aminosilane

Glass

B

| 8 | 710 | 658 | 685 | 650 | 661 |

Count density (molecules of Atto647N / field)

| Blank | After Atto647N-NHS incubation | After 16h wash buffer incubation | After DMF and methanol wash | After 1st Edman cycle | After 2nd Edman cycle |

Representative images

| Number of fields | 10 | 10 | 9 | 10 | 10 | 11 |

Supplementary Figure 5

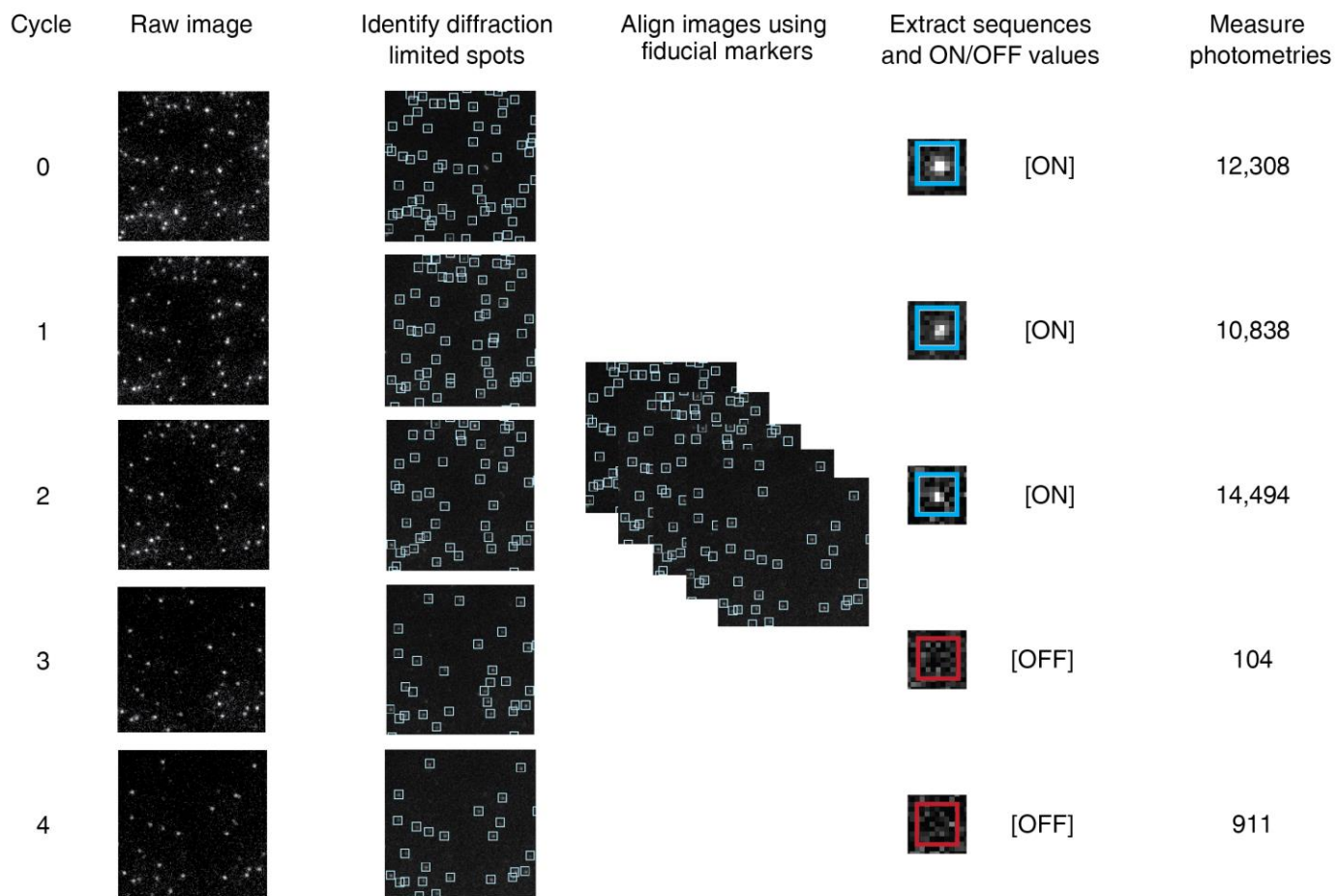The aminosilane surface is stable to Edman chemistry.

(**A**) Schematic of assay. A layer of APTES was covalently formed on a glass surface by siloxane bond formation (-Si-O-Si-). (**B**) Counts of single Atto647N-NHS fluorophores (plotted as mean count, shown above, per microscopy field +/- s.d.), immobilized *via* a stable amide linkage to the silane layer, remain unchanged with repeated experimental cycles of Edman chemistry and after washes with wash buffer.
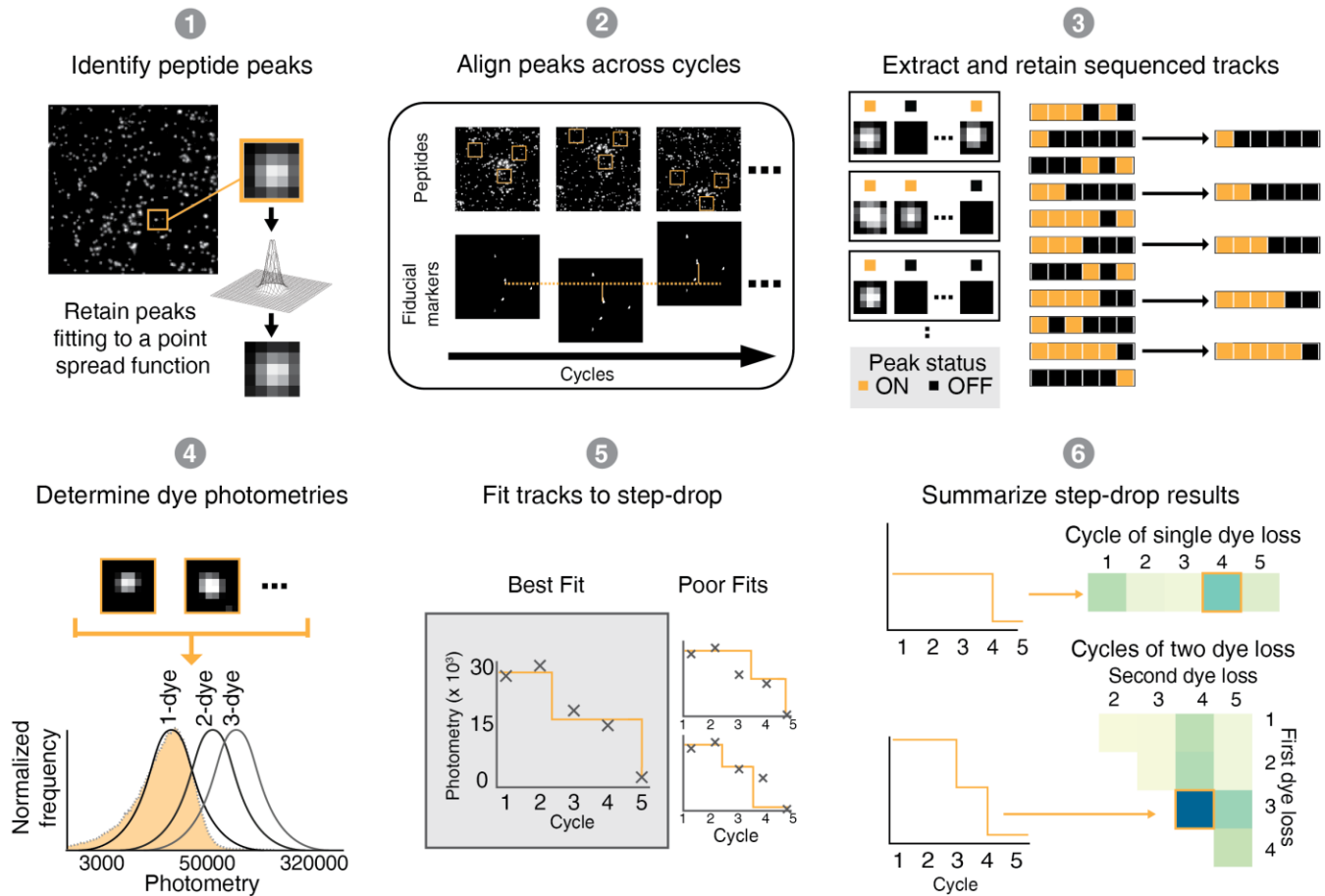
Supplementary Figure 6

Image-processing pipeline.

Overview of computational analysis to (**1**) identify fluorescent peptides as peaks in TIRF images, (**2**) align imaged peaks across consecutive Edman cycles, (**3**) identify the cycle at which each dye is removed, retaining "well-behaved" peptides. Dye positions are assigned using a maximum likelihood statistical model (see **Online Methods**), based on the empirical observation (**4**) that fluorescence intensities for one dye are log-normally distributed with a (log-normal) mean μ and standard deviation σ. Intensities for higher numbers of dyes are well-fit by log-normals with mean $\mu +$ ln(*dye count*) – dye-dye interaction factor Q_c , and standard deviation σ (**Supplementary Fig. 9**). (**5**) For each peptide, the number of dyes present after each Edman cycle is inferred by fitting observed intensities to each of the possible monotonically decreasing step functions (for up to 5 dyes), selecting the function maximizing a quality of fit scored using the lognormal probability density functions. (**6**) Counts of individual molecules exhibiting different step drop patterns are summarized in histograms.

Cycle	Raw image	Identify diffraction limited spots	Align images using fiducial markers	Extract sequences and ON/OFF values		Measure photometries
0					[ON]	12,308
1					[ON]	10,838
2					[ON]	14,494
3					[OFF]	104
4					[OFF]	911

Supplementary Figure 7

Image-processing summary.

Fluorescent spots were identified using a Gaussian peak fitting algorithm, then images were aligned between experimental cycles based on positions of fiducial markers. Each spot's position was extracted from the aligned images, with the spot categorized in each frame as either ON or OFF depending on the presence of a well-fitting peak. Spot intensities in each frame were then measured using Mexican hat photometry.

JF549 labeled (top) and
Atto647N labeled (bottom)
single peptide track
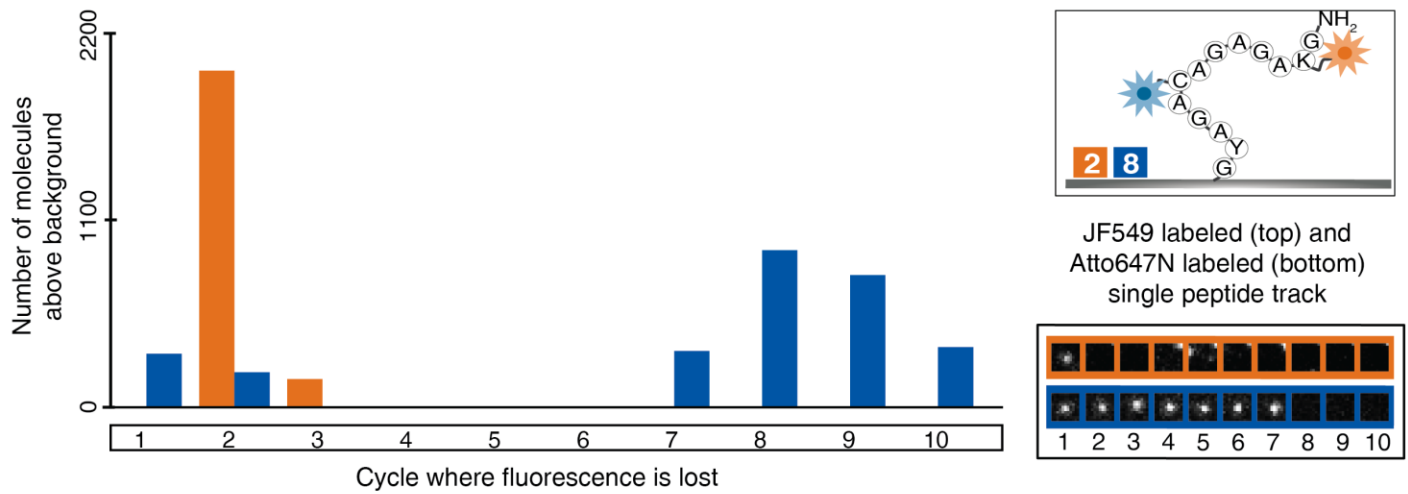
Supplementary Figure 8

The sequence positions of multiple amino acid types can be determined by labeling each type with a distinct dye.

The histogram displays counts of individual molecules of the doubly labeled peptide GK‡AGAGAC◆AGAYG (summarizing data from 400 image fields) indicating the Edman cycle numbers at which the two dyes were removed. An example of an individual doubly-labeled molecule is shown in the extracted TIRF images at bottom right. ‡ indicates Janelia Fluor 549 conjugated to lysine and ◆ indicates Atto647N conjugated to cysteine.

A

B

C
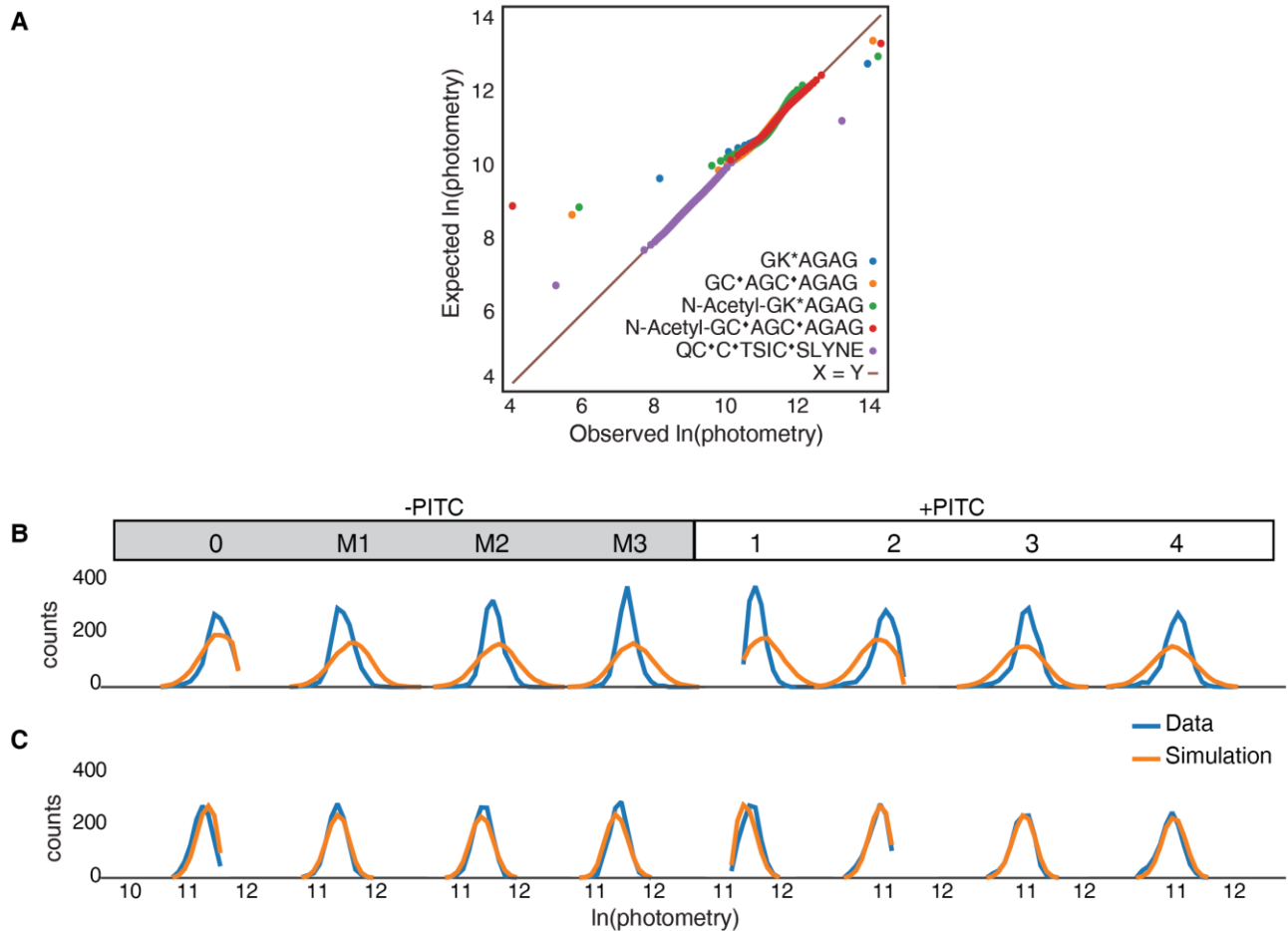
Supplementary Figure 9
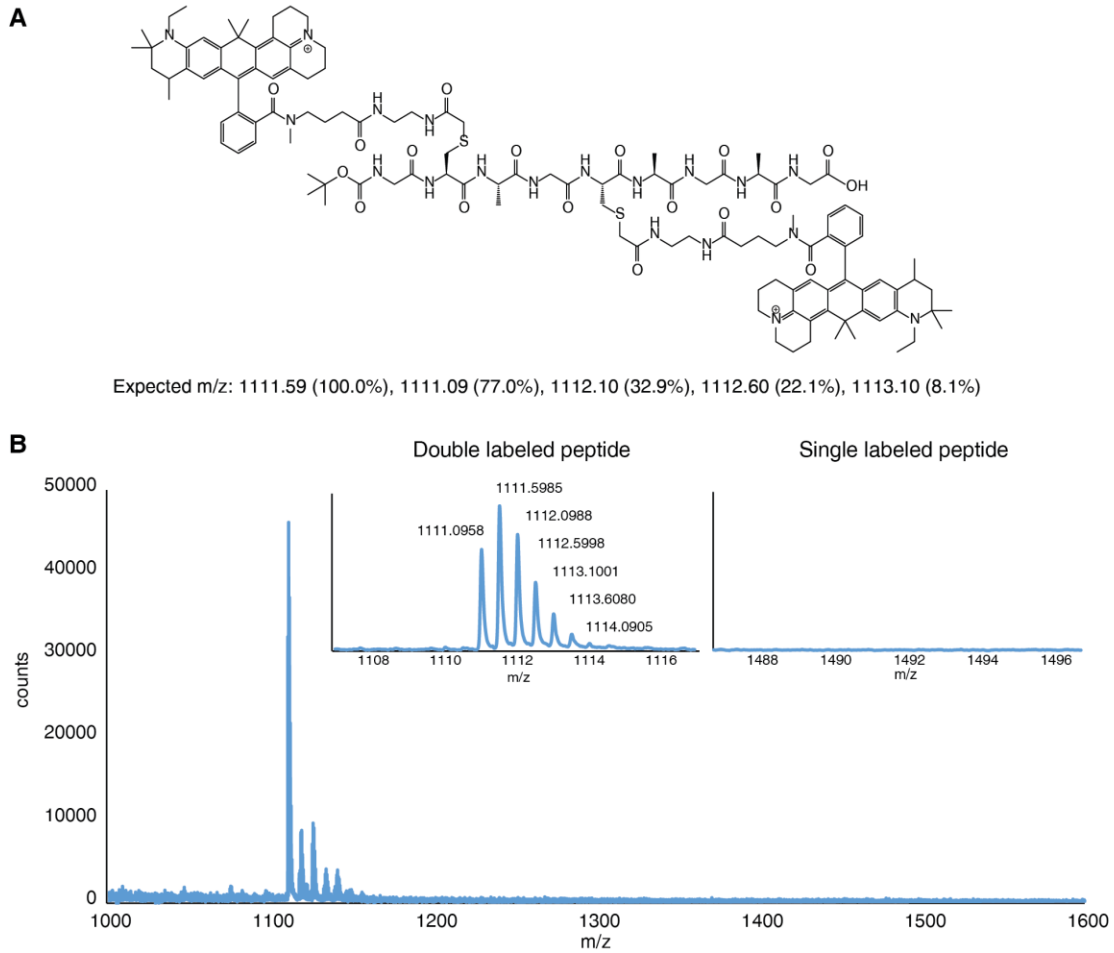
Measurement and modeling of fluorophore intensities.

(**A**) Fluorophore intensities follow a lognormal model. Photometries in the last frame before a dye labeled peptide permanently turns OFF predominantly represent the intensity of a single fluorophore, regardless of how many dyes a peptide initially started with. The distribution of these photometries is consistently lognormal across multiple experiments as shown by the Q-Q plot. Each point indicates a percentile of the lognormal photometry histogram of GK*AGAG, GC♦AGC♦AGAG, N-Acetyl-GK*AGAG, N-Acetyl-GC♦AGC♦AGAG, QC♦C♦TSIC♦SLYN with n=97137, n=273411, n=72905, n=155097 peptides, respectively. * indicates TMR conjugated to lysine ♦indicates Atto647N conjugated to cysteine. (**B, C**) Statistical models for photometry of multiple dyes were refined using forward simulation to optimize the values of the lognormal shape parameter σ^* and dye-dye interaction factor Q_c. Photometry distributions of peptides with the observed (blue) and simulated (orange) dye sequence: [2,2,2,2,2,1,1,1,0,0,0,0] for (**B**) a poor parameter choice, showing results of an overestimated σ^* and underestimated Q_c, and for (**C**) the optimized values of $\sigma^* = 0.20$ and $Q_c = 0.30$. Data shown for the initial condition, 3 mock cycles, and 4 Edman cycles, n=273411 peptides. The remaining cycles, with 0 dyes, are omitted.
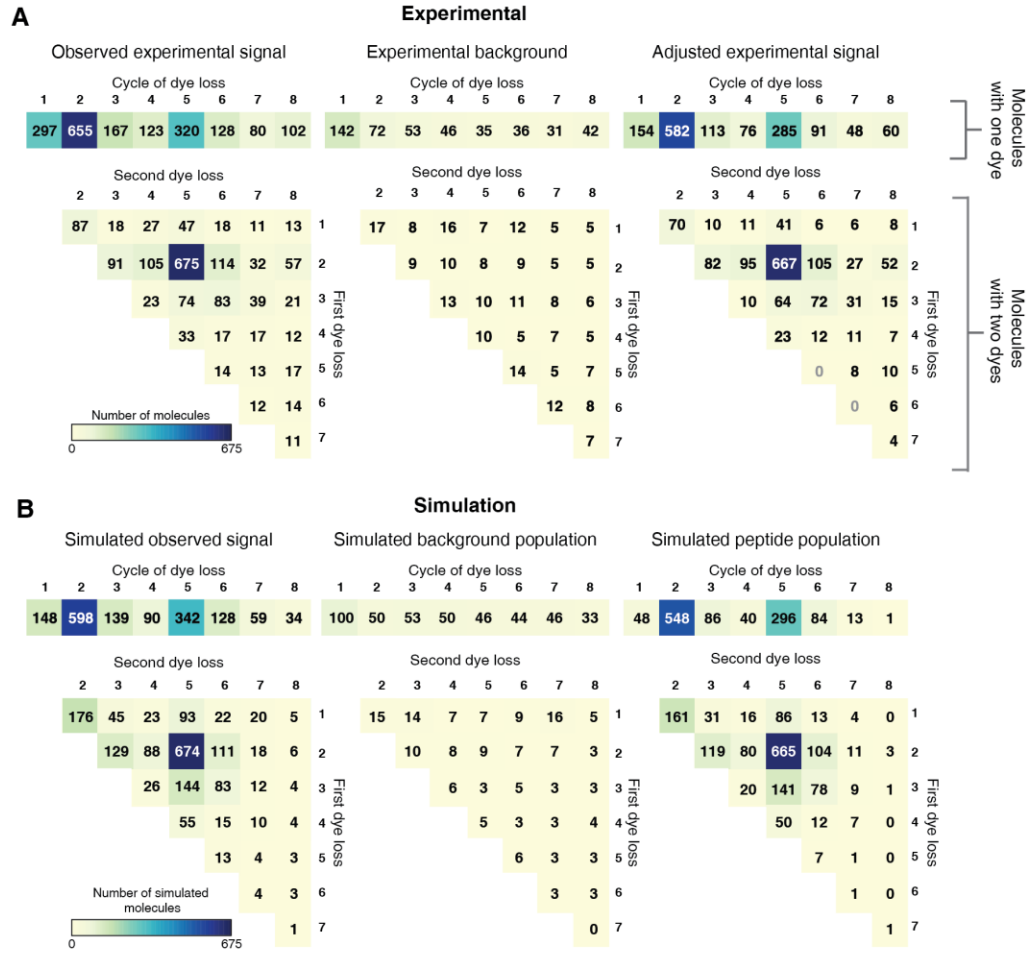
Supplementary Figure 10

Monte Carlo simulation of fluorosequencing closely matches the experimentally observed error distribution.

(**A**) Experimental sequence histograms of GC•AGC•AGAG (**A**, left panel) and its N-acetylated control (**A**, middle panel) replotted from **Fig. 4B** for easy comparison. (**B**) Simulated fluorosequencing of GC•AGC•AGAG with errors (**B**, right panel) and its N-acetylated control (**B**, middle panel) result in observed (simulated) signal (**B**, left panel) that closely matches observed experimental data in **A**. ◆ indicates Atto647N conjugated to cysteine.

A

Expected m/z: 1111.59 (100.0%), 1111.09 (77.0%), 1112.10 (32.9%), 1112.60 (22.1%), 1113.10 (8.1%)

B

Double labeled peptide

Single labeled peptide

1111.5985
1112.0988
1111.0958
1112.5998
1113.1001
1113.6080
1114.0905

Supplementary Figure 11

High-resolution mass spectrometry confirmation of the purity of the doubly labeled peptide GC◆AGC◆AGAG.

(**A**) Peptide structure with expected mass/charge (m/z) for its +2 charge state and top 5 isotopic variants. Single dye conjugates have expected m/z values of 1493.73 (+1 charge state). (**B**) High resolution mass spectrometry of the HPLC purified peptide confirms the presence of two Atto647N dyes. ◆indicates Atto647N conjugated to cysteine.
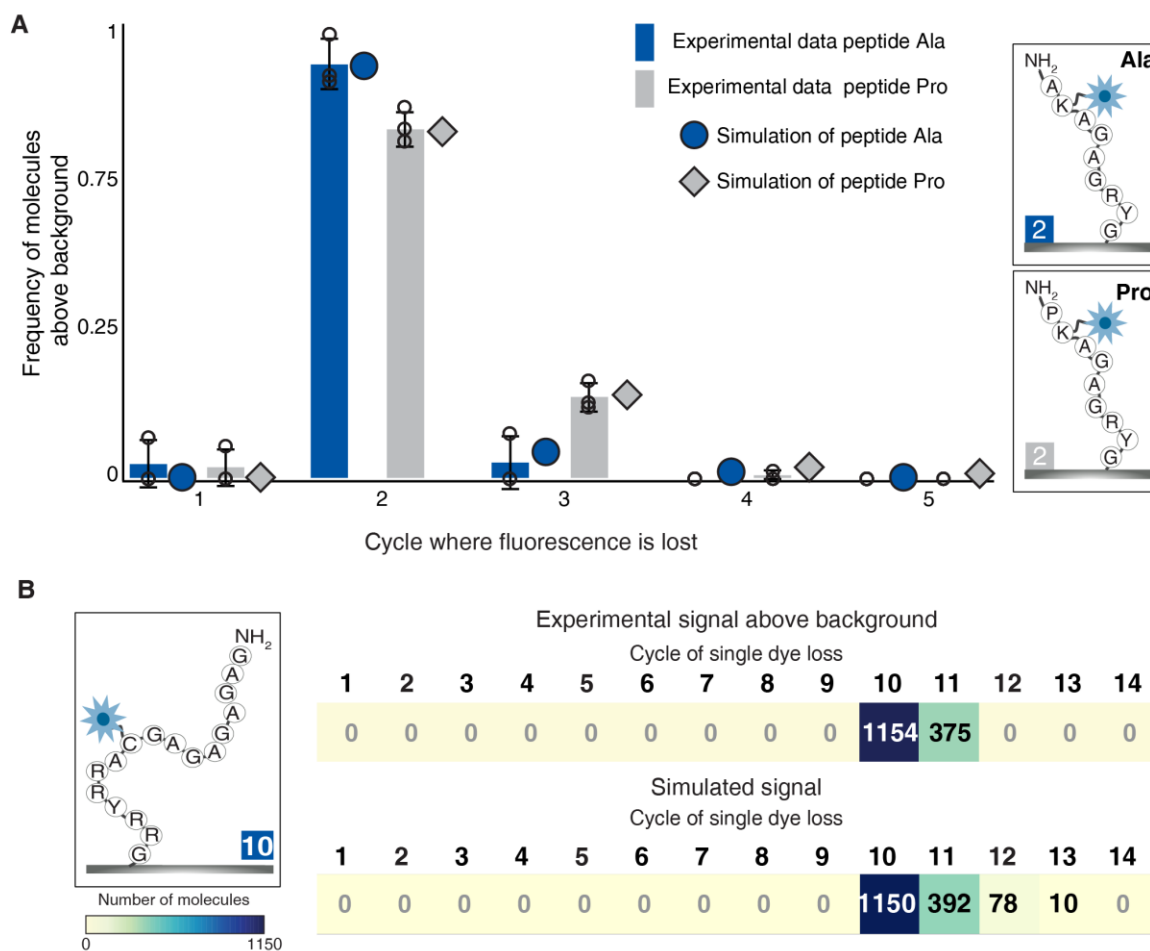
Supplementary Figure 12

Effects of peptide composition and length on Edman cleavage efficiencies.

(A) To better understand the range of Edman efficiency across amino acids we sequenced two synthetic peptides, differing only by the first amino acid, AK[†]AGAGRYG and PK[†]AGAGRYG. These were chosen for their historic ease, in the case of alanine, or difficulty, in the case of proline, of Edman sequencing[15]. Experiments were performed in triplicate (bar chart represents the mean +/- s,d. across experiments), sequencing both peptides simultaneously in a multiplexed flow cell, and results were averaged and compared with simulation to determine error rates. Error rates of 3% dye destruction, 30% surface degradation were identical across the two samples, while Edman cleavage efficiency was 95% and 91% for the alanine and proline samples respectively. **(B)** Consistent with the higher Edman cleavage efficiencies observed for alanine, a peptide composed of glycine/alanine repeats (GAGAGAGAGC[♦]ARRYRRG) with a fluorophore at the 10th position sequenced efficiently (top histogram, 400 fields) and was well fit by simulations with a 97% Edman cleavage efficiency, 3% dye destruction, and 4% surface degradation rate (bottom histogram). (Note that "dud" dye rates cannot be determined through simulation for singly labeled peptides.) † indicates Atto647 conjugated to lysine and ♦ indicates Atto647N conjugated to cysteine.
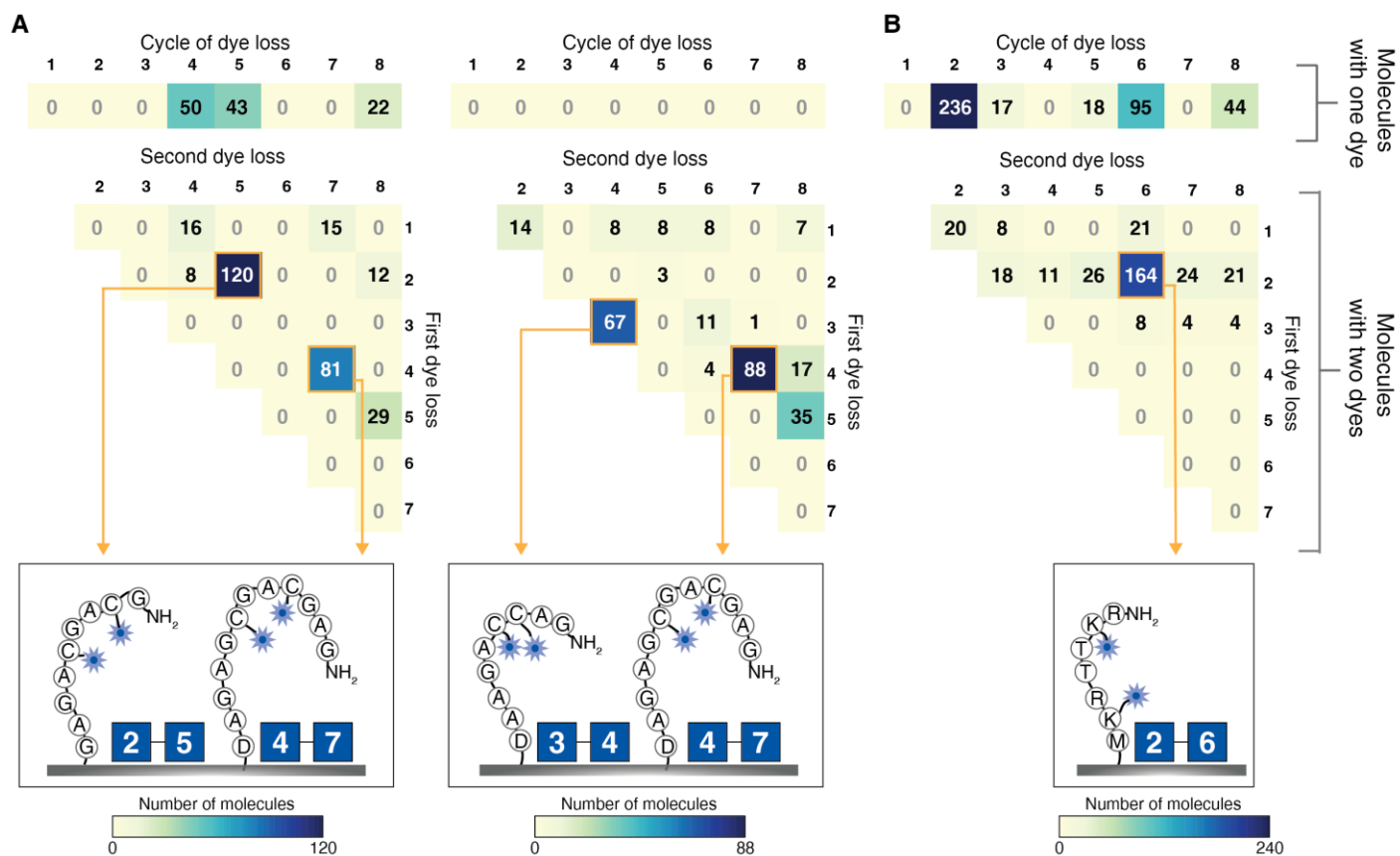
Supplementary Figure 13

Full one- and two-dye fluorosequencing histograms for peptides in Fig. 5a and Fig. 5d confirm signal for the expected sequence patterns.

(**A**) Histograms tallying counts of molecules sequenced from a mixture of GC•AGC•AGAG with GAGC•GAC•GAGAD (left panel, 98 fields) and GAC•C•AGAAD with GAGC•GAC•GAGAD (right panel, 49 fields) (**B**) Histograms of sequenced peptide RK†TTRK†M, 49 fields. ♦ indicates Atto647N conjugated to cysteine and † indicates Atto647N coupled to lysine residues.
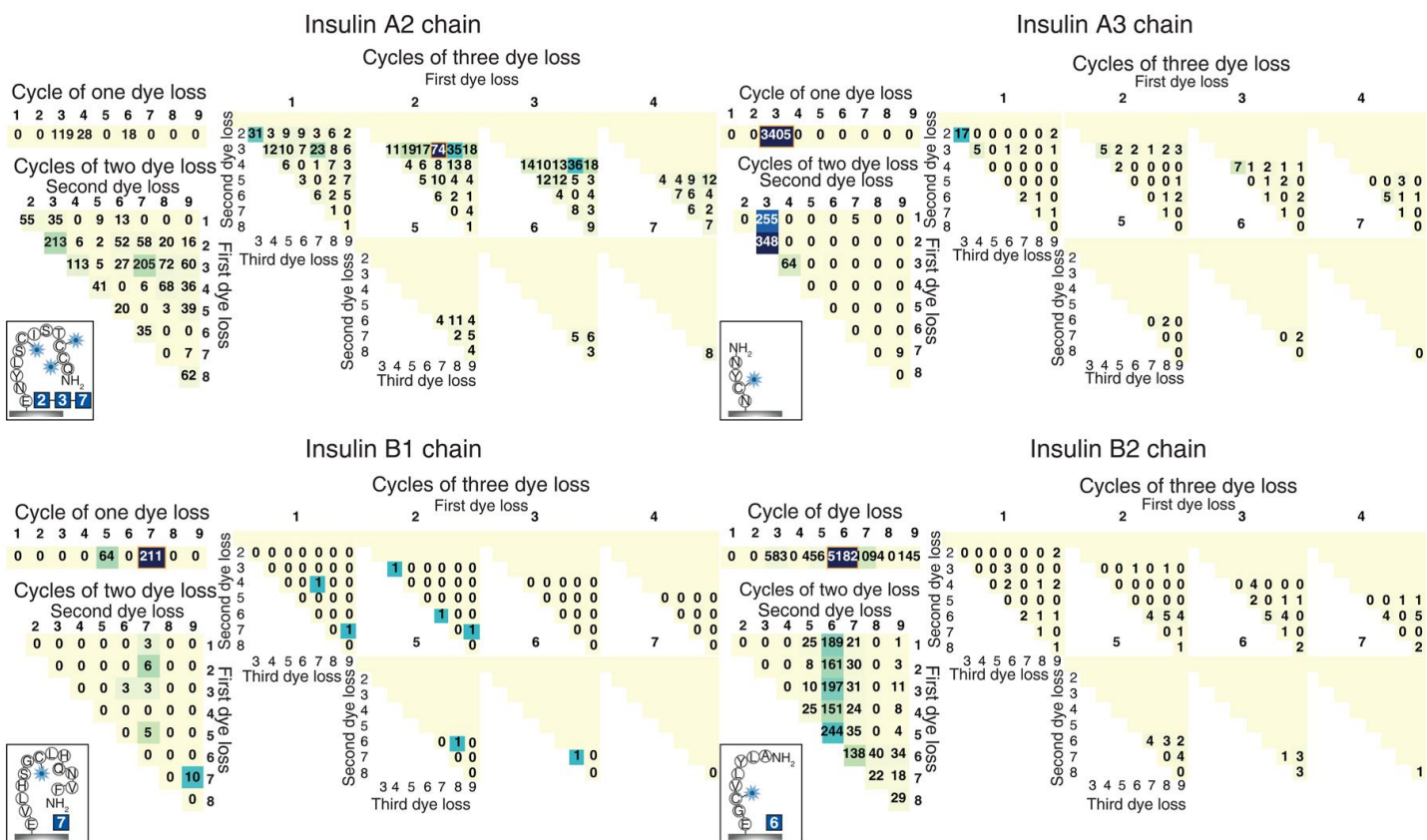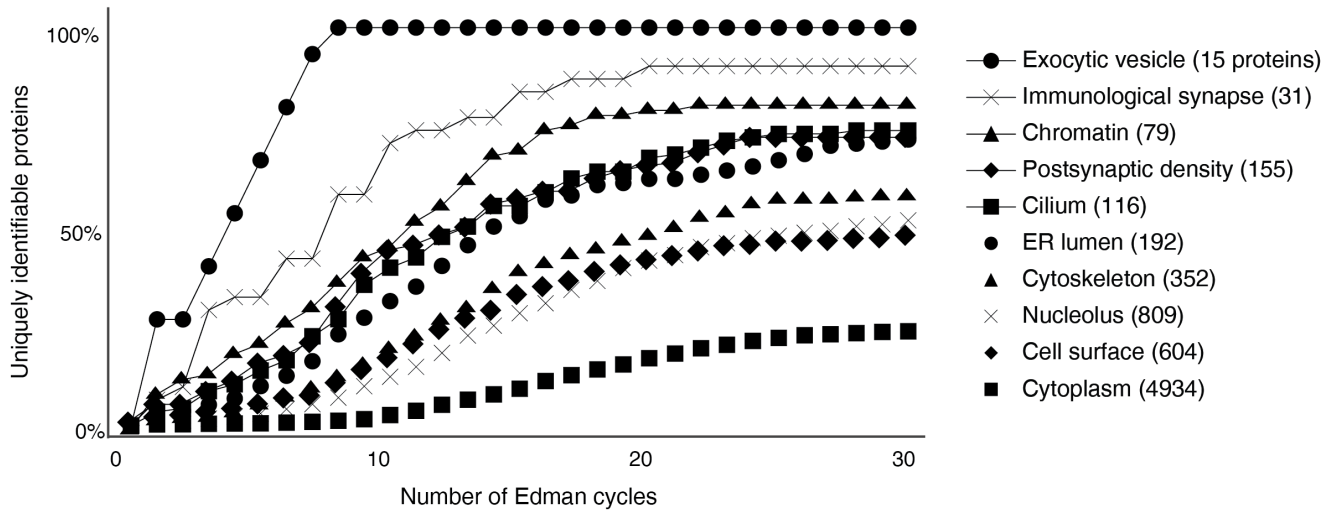
Supplementary Figure 14

One-, two-, and three-dye fluorosequencing histograms for insulin peptides (Fig. 5b) confirm signal for the expected sequence patterns.

Plotted are the background-adjusted one, two, and three dye histograms for insulin A2 chain (QC♦C♦TSIC♦SLYNE, measured across 100 image fields), A3 chain (NYC♦N, 120 fields), B1 chain (FVNQHLC♦GSHLVE, 72 fields), and B2 chain (ALYLVC♦GE, 100 fields), respectively. ♦ indicates Atto647N conjugated to cysteine.

Coverage of human proteins with two label types and expected errors

Legend:
- Exocytic vesicle (15 proteins)
- Immunological synapse (31)
- Chromatin (79)
- Postsynaptic density (155)
- Cilium (116)
- ER lumen (192)
- Cytoskeleton (352)
- Nucleolus (809)
- Cell surface (604)
- Cytoplasm (4934)

Y-axis: Uniquely identifiable proteins (0%, 50%, 100%)
X-axis: Number of Edman cycles (0, 10, 20, 30)

Supplementary Figure 15

Modeling the expected effects of experimentally determined error rates on protein identification.

The effects of experimental errors were modeled on the expected identification rates of sets of human proteins in the subcellular compartments examined in **Fig. 1C**. Each curve plots coverage of uniquely identifiable proteins, as a function of Edman cycles performed, considering the scenario of labeling only cysteines and lysines on peptides formed by GluC proteolysis, which cleaves after glutamate or aspartate, when considering error rates of 94% Edman cleavage efficiency, 5% dye destruction, 5% surface degradation, and 7% "dud" dyes. Modeling was performed using the Monte Carlo procedure of ref. 6. as described in **Online Methods**. Application to more complex samples in the future could potentially be achieved through reduction of these errors, introduction of additional amino-acid-specific labels, or a combination. The consecutive covalent labeling of Cys, Lys, Asp/Glu, Trp, and the amino terminus of model peptides has been reported[14], so there is no intrinsic barrier to extending the approach to additional amino acid types, provided the labels can be independently distinguished.